# The Role of Nozzle-Exit Conditions on the Flow Field of a Plane Jet

Ravinesh C. Deo

***Abstract*—**This article reviews the role of nozzle-exit conditions on the flow field of a plane jet. The jet issuing from a sharp-edged orifice plate at a Reynolds number ($Re$=18000) with nozzle aspect ratio ($AR$=72) exhibits the greatest shear-layer instabilities, highest entrainment and jet-spreading rates compared to the radially contoured nozzle. The growth rate of the shear-layer is the highest for the orifice-jet although this property could be amplified for larger $Re$ or $AR$. A local peak in turbulent energy is found at $x \approx 10h$. The peak appears to be elevated for an orifice-jet with lower $Re$ or $AR$. The far-field energy sustained by the orifice-jet exceeds the contoured case although a higher $Re$ and $AR$ may enhance this value. The spectra displays the largest eddies generated by the contoured nozzle. However, the frequency of coherent eddies is higher for the orifice-jet, with a larger magnitude achievable for lower $Re$ and $AR$.

***Keywords*—**Plane jet, Reynolds number, nozzle-exit conditions, nozzle geometry, aspect ratio.

## I. Background

THE classical belief that turbulence forgets its origin were common in the 20th century [1]. This perspective persisted because the properties of turbulent shear flows become invariant when normalized by a suitable velocity, scalar or length scale [Figs. 1-3; 2]. Thus the effect of exit-conditions decay with axial distance and is eliminated eventually. A shortfall of this understanding was the failure to recognize the dependence of the normalizing parameter itself (e.g. jet-width) on nozzle exit-conditions. Since the pioneering investigation by George [3], experimental, numerical and modeling studies have been used to dispel the classical theory of turbulence. Subsequently, the number of investigations on self-preservation and its independence from nozzle-exit conditions has continued to grow. The present article adds new information to these efforts by reviewing a set of three prescribed nozzle-exit conditions on flow characteristics using the case of a plane jet.

One particular free shear flow chosen to study the effects of nozzle-exit conditions is a plane jet. The jet is generated by a slender nozzle measuring $w \times h$ where $w$ and $h$ are oriented along the spanwise ($z$) and lateral ($y$) coordinates. The flow statistics are independent of the $z$-coordinate, so that the flow is considered statistically two-dimensional. There are several experimental, numerical and analytical investigations that advocated modern ideas of self-similar states for different nozzle-exit conditions [4]–[11]. The prime motive of all these studies was to verify the validity, or otherwise, of self-similar states relative to disparities in exit conditions. However, these studies focused on a single nozzle-exit condition or a set of systematically varying conditions, but an inter-comparison of the importance of one condition relative to another has not been evaluated.

Nozzle-exit conditions are conventionally defined by the jet-exit Reynolds number ($Re \equiv U_b h/\upsilon$) with $U_b$ = mean exit mean velocity and $\upsilon$ = kinematic viscosity), exit velocity and turbulence intensity profiles, nozzle aspect ratio ($AR = w/h$), nozzle-exit geometry, density ratio of jet fluid to ambient fluid and boundary conditions (e.g. sidewalls along the $x$-$y$ plane). In experiments, the common geometries used are sharp orifice plates [12], smooth contoured profile based on sinusoidal curves [13] or radially contoured profile based on a radial curvature [7]–[14]. The first case produces a saddle-backed profile while the others, a top-hat. The chosen aperture can be a long pipe or circular, triangular, elliptic or rectangular shapes. The shape is also known to impact the exit turbulence levels and mean velocity profiles. However, other parameters, such as $Re$ and $AR$ also influence the exit-boundary layer and the downstream mixing fields [15].

In spite of voluminous work on the impact of a single exit conditions on the entrained flow, the dominant role of one condition relative to another remains unexplored. This issue is stimulating for designers as changing one parameter (e.g. $Re$) while keeping the other constant (e.g. $AR$ or nozzle shape) inevitably moderates the mean velocity and turbulence intensity profiles [10], [16], [17]. Similar effects manifest in the boundary layer if the $AR$ or geometry is changed without altering $Re$ [6]–[10]. The secondary effects induced into the flow forbid the isolation of the impact of a particular condition in consideration.

From practical viewpoints, nozzles are chosen according their application so detailed understanding of the effect of a condition is crucial. For example, a contoured nozzle that produces a Blasius profile and laminar state at the exit minimizes pressure drop in supply pipes [18]. A pipe-jet with a fully-developed flow is easy to manufacture and is advantages in chimneys and stacks [19]. A nozzle with a sharp-edged orifice and a vena contracta enhances near-field mixing [18]. Industrial flows require high Reynolds number to generate broad range of eddies [20], while the breakup of eddies in pressure sprays is influenced by the rapidity of flow development and exit turbulence [21]. Thus, knowledge of the turbulent properties of jets with various initial conditions is useful for a greater understanding of the role of any given condition relative to another.

Dr. RC Deo is a Lecturer in Applied Mathematics in the School of Agricultural, Computational and Environmental Sciences, University of Southern Queensland (Springfield) Australia (phone: +61(07) 38078861; fax: +61(07) 38078861; correspondence e-mail: ravinesh.deo@usq.edu.au).

To our best knowledge, no prior study has considered the relative and inter-dependency of different nozzle-exit conditions on the turbulence properties of the propagating jet. In this article, we revisit our previous work on the effect of Reynolds number, aspect ratio and geometry [6]–[8], [10], [23]. Our aim is to examine the dominant or the overall effect of the three prescribed exit-conditions on flow dynamics and provide new information on statistical behaviors and underlying turbulence structures.

## II. Experimental Design

### A. Jet Facility, Nozzle Design Parameters and Conditions

The experiment has been detailed in [6]. Data were collected in the Fluids Laboratory at the School of Mechanical Engineering at The University of Adelaide. Unheated air was supplied by an open circuit wind tunnel driven by a variable-speed, 14.5 kW aerofoil-type centrifugal fan. The wind tunnel flow was pre-conditioned by a diffuser, settling chamber, honeycomb and screens, feeding a large, polynomial contraction where a series of plane nozzles where clamped securely.

The parallel sidewalls were flushed with the short sides of the slot ($h$) and aligned along the $x$-$y$ plane (Fig. 2 (b)). The sidewalls extended 2000 mm downstream (along the $x$-direction) and 1800 mm vertically (along the $y$-direction) to enhance the two-dimensionality of the emerging jet flow. Both walls were secured tightly by bolts to the ceiling to avoid acoustic disturbances. Table I lists the design parameters and the prescribed exit conditions. For each case tested, separate nozzles were constructed using two perspex plates consisting of a slot height ($h$) along the y-direction and slot width ($w$) along the $z$-direction of the nozzle. The prescribed exit conditions were as follows.

Case A tested the effect of $Re$ on a jet issuing from a planar nozzle with $h$ = 5.6 and $w$ = 340 mm corresponding to $AR$ = $w/h$ = 60. A reasonably large aspect ratio was necessary to produce a statistically two-dimensional jet far in the self-preserving region [8]. The upstream edge of the plates were machined with a radial contraction $r$ = 12 mm with the contraction factor, $r^* = r/h \approx 2.14$. This contraction was adequate to produce a Blasius mean exit velocity profile [7]. To achieve the required Reynolds numbers, the fan speed was varied systematically to produce flow rates ($Q$) over the range $7.6 \times 10^{-3} \leq Q \leq 8.4 \times 10^{-2}$ m$^3$s$^{-1}$ corresponding to $Re$ =1 500 – 16500 while the aspect ratio and nozzle geometry remained invariant.

In Case B, nozzles of various aspect ratios (very low to reasonably high) were constructed by shifting the sidewalls outwards to achieve $w$ = 150 – 720 mm resulting in $AR$ = 15 – 72. For all cases tested, $h$ = 10 and $r$ = 36 mm so that the contraction factor, $r^*$ = 3.60 resulted in a Blasius mean velocity profile [8]. For this case, all measurements were conducted at a flow rate, $Q = 1.944 \times 10^{-1}$ m$^3$s$^{-1}$ that corresponded to $Re = 1.80 \times 10^4$.

Case C examined the effect of geometry by systematically changing the nozzle contraction factor from $r^*$ = 4.5 – 36. The values of $r^*$ were incremented by a factor of two per step. For these nozzles, $h$ = 10 mm and $w$ = 720 mm was used to that a comparably large $AR$ = 72 was achieved. The step increment of r* produced four radially contoured nozzles, $r^*$ = 0.45, 0.90, 1.80 and 3.60. A fifth case with $r^*$ = 0 was obtained by reversing the orientation of the plates for $r^*$ = 0.45 with the sharp end facing upstream. This case resembled orifice plates in previous studies [12], [24]–[25]. Due to the significant differences in $r^*$ (thus, the geometry), the mean exit velocity profiles exhibited various shapes ranging from saddle-back ("$M$" shape) to top-hat (Blasius) shape (Table I, Case 3). For all cases, the flow rate was kept fixed at $Q = 1.944 \times 10^{-1}$ m$^3$s$^{-1}$ corresponding to $Re = 1.80 \times 10^4$. For more details on the nozzle designs for the three prescribed nozzle-exit conditions, the reader is referred to [6].

### B. Hot Wire Anemometry and Data Acquisition System

For all measurements, a constant temperature anemometer and single hot-wires were used. In accordance with Brunn [26], custom-designed sensors were chosen to minimize heat loss from the end points. The length $l_w$, and diameter $d_w$ was chosen based on literature. References [27] and [28] used $l_w/d_w$ = 208 and 160, respectively to resolve fine-scale turbulent structures. Reference [29] states that heat loss from the sensor is 15% when $l_w/d_w$ = 200 and the anemometer is operated at an overheat of 1.0. Bearing in mind that $l_w$ and $d_w$ are critical hot-wire parameters, we chose a set of copper-plated tungsten wires of $l_w$ =1 mm and $d_w$ = 5 μm to achieve the ratio $l_w/d_w$ = 200.

The anemometer was operated at overheat ratio of 1.5 to provide the sensor adequate sensitivity while reducing the heat losses from its ends. A 3-dimensional traverse enabled measurements laterally (across) and axially (streamwise) of the propagating jet. The static pressure measurements were made with separate Pitot static tubes for calibrating the probe. The streamwise component of instantaneous velocity signals, $U(x)$ were measured on the jet centerline while the lateral components, $U(x, y)$ were measured at selected $x/h$ across the jet at the three prescribed nozzle-exit conditions (Table I, A-C).

A PC-30F system attached to a PC was utilized for measurements. This system was a 200 kHz multi-channel analogue to digital converter with a 12-bit (2.4 mV) resolution. After monitoring real-time signals on a Tektronix Oscilloscope, data were visualized in WaveView 2.0 (DOS based software) for preliminary check. The input range of system was ± 5.0V, so an appropriate offset was applied to the sampled voltage to rectify the signal within ± 3.0 V. This avoided clipping the tails of fluctuating velocity [30]. A square wave test set the response frequency of the system to 15 kHz. A cut-off frequency, $f_c$ = 9.2 kHz was used to sample data at a Nyquist frequency of 18.4 kHz for 22.4 seconds per location. The ranges of measurements were $0 \leq x/h \leq 160$ for Cases A and B ($Re$ and nozzle geometry experiments) and $0 \leq x/h \leq 85$ for the experiment on $AR$.

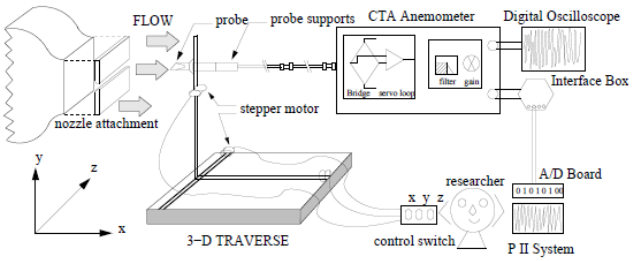


Fig. 1 The experimental scheme showing the present nozzle attachment to the wind tunnel exit and the hot wire and data acquisition system (Reproduced after Deo [6])

## III. Results and Discussion

### A. Jet Definitions and Nozzle-Exit Conditions

Table I summarizes the nature of the exit flows generated by the three prescribed conditions. In Case A, the jet measured from radially contoured geometry ($r^*$ = 2.14) with the smallest Reynolds number ($Re$ = 1500) and large aspect ratio ($AR$ = 60) exhibited the highest shear-layer turbulence intensity (~6.5%). By contrast, its momentum thickness-based Reynolds number ($Re_\theta$) is the smallest (~1031) compared to $Re_\theta$ = 6537 for the case $Re$ = 16500. This indicates that a low Reynolds number jet is characterized by a thicker and perhaps, a more unstable shear layer at the nozzle-exit.

When measured at a high Reynolds number ($Re$ = 18 000) using a contoured geometry ($r^*$ = 3.60) and various nozzle aspect ratios (Case B), the initial flow does scale with nozzle aspect ratio. Thus, an initial turbulence intensity of ~13% is achieved within the shear-layer of a jet with $AR$ = 15 compared to ~5% for $AR$ = 72. Correspondingly, the momentum-based Reynolds is nearly three times larger for the former jet. Based on this, it is hypothesized that a nozzle constructed with a small aspect ratio could exhibit greater disturbance in its shear-layer. If so, this could supports greater three-dimensional effects for a low-$AR$ jet presumably induced by the sidewalls that enclose the plane jet. However, if a low Reynolds number (e.g. $Re$ = 1500) is used, further instabilities could be fed in as evident from Case A.

Case C highlights the effect of nozzle geometric factor ($r^*$) whereby $Re$ = 18000 and $AR$ = 72 was used. Recall that if the $r^*$ is >2.0, the jet resembles to one from a contoured nozzle. It appears that $r^*$ has a significant effect on the initial turbulence intensity and the shape of the mean velocity profiles. Table I demonstrates unambiguously that the mean and the turbulent properties are modified dramatically if the nozzle geometry is altered from a sharp-edged orifice ($r^*$ = 0) to a radially contoured case ($r^*$ = 3.60). This also moderates the shape of the velocity profile from a saddle-back to a top-hat (uniform) profile as reported previously [7]. Following the increase in $r^*$, the initial shear layer turbulence intensity decreases from ~22% to ~3.9%, with a retrospective increase in $Re_\theta$ for jets with large values of $r^*$.

However, if a smaller $Re$ and $AR$ is used, the jet issuing from the orifice plate may produce much larger initial turbulence intensity but a significantly smaller $Re_\theta$.

Accordingly, the analysis confirms that for any given plane jet, a highly disturbed and a relatively thin initial shear layer is achieved by employing a sharp-orifice plate constructed with a small aspect ratio. This shear layer is expected to be very thin (i.e. with relatively small $\delta_m$ and $\theta_m$) and significantly unstable as verified by investigations on round [18] and plane [7] jets. Additionally, the disturbance in the initial shear layer may be enhanced if the Reynolds number is reduced. In comparison to the other conditions, the nozzle geometric factor appears to have the greatest impact on the initial region of the jet by directly moderating the mean exit velocity and turbulence intensity profiles.

### B. Mean Flow Properties

In accordance with the principles of similarity, the centerline velocity $U_c(x)$ for a plane jet is known to meet

$$U_c(x)/U_b \approx x_p \tag{1}$$

between $x/h$ = 0 – 6,

$$U_c(x)/U_b \approx [K_u(x/h + x_{01}/h)]^{-1/2} \tag{2}$$

and jet half-widths follow

$$y_{0.5}(x)/h \approx [K_y(x/h + x_{02}/h)] \tag{3}$$

in the self-preserving field. Here $U_b$ = bulk mean exit velocity, $y_{0.5}(x)$ is jet-half width deduced from lateral profiles of the mean velocity, $U(x, y)$, $K_u$ and $K_y$ = jet decay and spreading rates, $x_{01}$ and $x_{02}$ = virtual origin, $x_p$ = length of the potential core. Given the demonstrated disparities in the exit flows of the prescribed jets, the properties arising from (1)–(3) are expected to evolve independently for the downstream flows.

Fig. 2 plots $x_p$ (*a-c*) and the ratio of $U(x, y)$ and $U_c(x)$ (2*d-f*) measured in the near field at $x/h$ = 3. Evidently, the trends in the potential core lengths are opposite for Case A ($Re$-effect) and Case B ($AR$-effect). That is, in Case A, $x_p$ is a decreasing function of $Re$, whereas in Case B, it presents as an increasing function of $AR$. The shorter potential core for a jet measured at the small aspect ratio ($AR$ = 15) agrees with higher three-dimensional effects leading to greater distortions in the large-scale eddy structures. Ref [31] used very small $AR$-elliptic jets to demonstrate 3-8 folds greater mass entrainment compared to the high-$AR$ jets. For cases with small-$AR$, the azimuthally distorted vortices are known to increase the interfacial area to facilitate active engulfment of ambient fluid into the mixing layers. This potentially results in higher near-field spreading rates for low-$AR$ jets compared to their high-$AR$ counterparts. To verify these trends, Fig. 2 (d)-(e) shows the highest spreading rate for jet with largest Reynolds number, but measured at the small aspect ratio.

As confirmed previously [e.g. Ref 7], potential core in the orifice-jets ($r^*$ = 0 & 0.45) were nearly absent. Thus, they are denoted as $x_p \approx 0$ (Fig. 2 (f)). This has been verified by the decay of $U_c(x)$ for the orifice-jet (not shown here) where sudden expansion of the jet fluid occurred at $x/h$ = 2, and thus

prohibited the formation of a constant velocity region. The increased distortion of $U_c(x)$ supports a vena contracta for a sharp-edged orifice as reported for plane, rectangular and round jet flows [7]; [18]; [32]. This finding accord to [31] that instability frequencies scale with the thinnest momentum thickness and is associated with maximum vorticity and higher entrainment rates for the orifice. However, for $r^* \geq 0.90$, the magnitudes of $x_p$ increased from $\approx 1h$ to $4h$, and is confirmed by the decay of $U_c(x)$. In comparison to Cases A and B, the results suggest that the near-field entrainment is enhanced for a jet issuing from a sharp-edged orifice geometry measured at small aspect ratio and high Reynolds number.

In accordance with [31], instability frequencies in elliptical jets scale with their initial momentum thickness. This indicates that for a jet with smaller displacement thickness of the mean exit velocity profile, the instability mechanism is associated with high vorticity in the shear-layer. From this stand point, a higher entrainment rate for the orifice ($r/h \leq 0.90$) relative to a lower value for the radially contoured cases ($r/h > 1.80$) is probably driven by the differences in the initial boundary layer thickness (Table I).

TABLE I
PRESCRIBED CASES FOR NOZZLE-EXIT CONDITIONS

**CASE A**: EFFECT OF REYNOLDS NUMBER ($AR = 60$, RADIALLY CONTOURED EXIT $r^* = 2.14$, JET CONFIGURED WITH SIDEWALLS (2-DIMENSIONAL)

| *Re* | δ | θ | *H* | $Re_\theta$ | $u'_p/U_c$ | *Nature of Mean Exit Velocity Profile* |
|---|---|---|---|---|---|---|
| 1500 | 0.133*h* | 0.068*h* | 1.95 | 1031 | 6.5 | |
| 3000 | 0.116*h* | 0.056*h* | 2.09 | 1709 | 6.0 | |
| 4200 | 0.113*h* | 0.050*h* | 2.35 | 2105 | 5.2 | nearly top-hat |
| 7000 | 0.109*h* | 0.045*h* | 2.43 | 3154 | 4.0 | |
| 10000 | 0.098*h* | 0.040*h* | 2.45 | 4038 | 2.0 | |
| 16500 | 0.097*h* | 0.039*h* | 2.49 | 6567 | 1.5 | |

**CASE B**: EFFECT OF NOZZLE ASPECT RATIO NUMBER (RE = 18 000, RADIALLY CONTOURED EXIT $r^* = 3.60$, JET CONFIGURED WITH SIDEWALLS (2-DIMENSIONAL)

| *AR* | δ | θ | *H* | $Re_\theta$ | $u'_p/U_c$ | *Nature of Mean Exit Velocity Profile* |
|---|---|---|---|---|---|---|
| 15 | 0.190*h* | 0.081*h* | 2.34 | 1488 | 13.0 | |
| 20 | 0.172*h* | 0.072*h* | 2.38 | 1322 | 11.1 | |
| 30 | 0.155*h* | 0.065*h* | 2.39 | 1194 | 11.0 | nearly top-hat |
| 50 | 0.101*h* | 0.040*h* | 2.52 | 735 | 6.8 | |
| 60 | 0.088*h* | 0.035*h* | 2.51 | 643 | 6.1 | |
| 72 | 0.072*h* | 0.029*h* | 2.49 | 533 | 6.0 | |

**CASE C**: EFFECT OF NOZZLE GEOMETRY (RE = 18 000, $AR = 72$, JET CONFIGURED WITH SIDEWALLS (2-DIMENSIONAL)

| *r** | δ | θ | *H* | $Re_\theta$ | $u'_p/U_c$ | *Nature of Mean Exit Velocity Profile* |
|---|---|---|---|---|---|---|
| 0 | - | - | - | - | 22 | enhanced saddle back |
| 0.45 | 0.054*h* | 0.030*h* | 1.80 | 551 | 17 | saddle-back |
| 0.90 | 0.068*h* | 0.035*h* | 1.95 | 642 | 8.0 | |
| 1.80 | 0.127*h* | 0.052*h* | 2.44 | 955 | 5.5 | top-hat |
| 3.60 | 0.151*h* | 0.061*h* | 2.95 | 1120 | 3.9 | |

Notes:
- δ and θ are displacement thickness of the initial shear-layer.
- $H$ – shape factor of the mean exit velocity profile
- $Re_\theta$ = exit-momentum-based Reynolds number
- $u'_p / U_c$ is the shear-layer turbulence intensity at the nozzle exit plane.

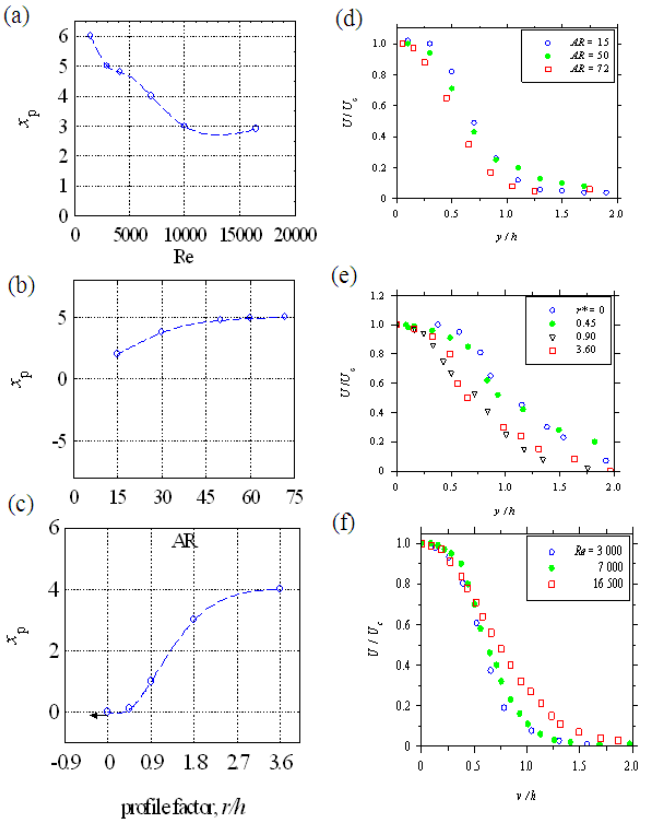


Fig. 2 The effect of nozzle-exit conditions in near-field at $x/h = 3$. (a) lengths of potential core ($x_p$) (left panel, a-c); (b) lateral profiles of the mean velocity $U(x, y)/U_c(x)$ (right panel, d-f) (Redrawn after Refs [10], part (a); Ref [8], part (b); Ref [7], part (c)

Fig. 3 displays the jet decay and spreading rates for the three prescribed nozzle-exit conditions deduced from our previous investigations [7]–[8], [10]. Following the trends in $x_p$, opposite trends are noted for $K_u$ and $K_y$ between the Cases A and B. That is, as *Re* is increased, the magnitudes of $K_u$ and $K_y$ decrease asymptotically. By contrast, these values decrease with increased *AR*. These trends are consistent with high entrainment rates for the low *Re* and high-*AR* jet. However, contraction profile factor seeds an opposite effect whereby the $K_u$ and $K_y$ values are the largest for the orifice compared to the contoured nozzle. It is thus clear that the far-field entrainment rates are enhanced by using a sharp-edged orifice nozzle with a large aspect ratio and small Reynolds number.

A very useful property of turbulent jets is their ability to entrain the ambient fluid as this may reflect their efficiency in mixing two fluids (e.g. fuel and air in a combustion chamber). Thus, a good understanding of how this constraint depends on nozzle-exit conditions is necessary, especially for designing mixing devices. The entrainment rate, $E$ is usually measured by the mass flow rate, $m(x)$, at any $x$ relative to the initial value $m_o$ ($x = 0$). Since the jet spreads laterally, $E$ may be quantified by

$$E \equiv \frac{m(x)}{m_o} = \frac{1}{hU_b}\int_{-\infty}^{+\infty} U(x,y)\,dy \tag{4}$$

and the relations $m(x) / m_o \sim U_c(x)/U_b$ and $U_c(x) \sim x^{-1/2}$ yield

$$\left(\frac{m(x)}{m_o}\right)^2 = K_m\left(\frac{x-x_{04}}{h}\right) = K_m\,\xi \tag{5}$$

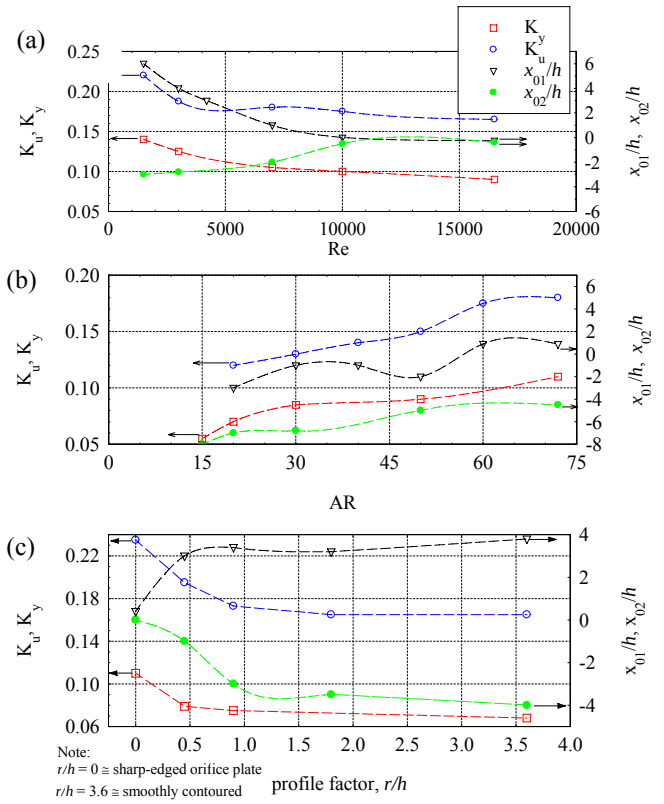


Fig. 3 Effect of nozzle-exit conditions on decay rate ($K_u$) and virtual origin ($x_{01}/h$) based on axial velocity profiles, jet spreading date ($K_y$) and virtual origin ($x_{02}/h$) based on lateral velocity profiles. (a) $Re$ = 1500 – 16500 ($AR$ = 60, $r^*$= 2.1), (b) $AR$ = 15 – 72 ($Re$ = 18 000, $r^*$= 3.60), (c) $r^*$ = 0 – 3.60 ($Re$ = 18 000, $AR$ = 72) (Redrawn after Refs [10], part (a); Ref [8], part (b); Ref [7], part (c)

In (5), $K_m$ measures of the entrainment rate due to the large-scale mean flow. Likewise, boundary layer thickness $\delta(x)$ may be estimated numerically for any $x$ by integrating $U(x, y)$ as

$$\delta(x) = \int_{y=0}^{y=\infty}\left(1-\frac{U(x,y)}{U_c(x)}\right)dy \tag{6}$$

Since $U_c(x) \sim x^{-1/2}$ and $y_{0.5}(x) \sim x$, it follows that $\delta(x)$ should vary as $x$ to yield

$$\delta(x)/h = K_\delta\left(x/h + x_{03}/h\right) \tag{7}$$

where $K_\delta$ represents the growth rate of the boundary layer along the streamwise direction and $x_{03}$ is the virtual origin.

Fig. 4 presents the entrainment rates ($K_m$) and virtual origins ($x_{04}$) depicted by (5). It is not surprising to note that the trends of $K_m$ for Cases A and C follow that of $K_u$ and $K_y$ (Fig. 3) although for Case B, they are opposite. In general, $K_m$ decreases asymptotically with increasing $Re$ and $r^*$, however, it increases for increased $AR$. This apparent discrepancy is explained by revisiting the jet half widths (not shown here).

In our earlier work [8], we showed that a jet with $AR$ = 15 and 20 exhibited significant three-dimensional effects due to very low aspect ratio. Thus the spreading rate for the low-$AR$ jets was amplified for $x$ = 10 – 30$h$. As $K_m$ is a secondary property computed from the profiles of the mean velocity, this anomaly could contribute to significant errors in estimating its magnitude. However, based on Cases A & C, the entrainment rate of a low $Re$-jet measured using a sharp-edged orifice ($r^*$ = 0) may entrain the ambient fluid more effectively than a high $Re$-jet issuing from a contoured geometry. Additionally, the virtual origins ($x_{05}$) follow similar patterns with generally decreasing values for increased $Re$ and $r^*$.

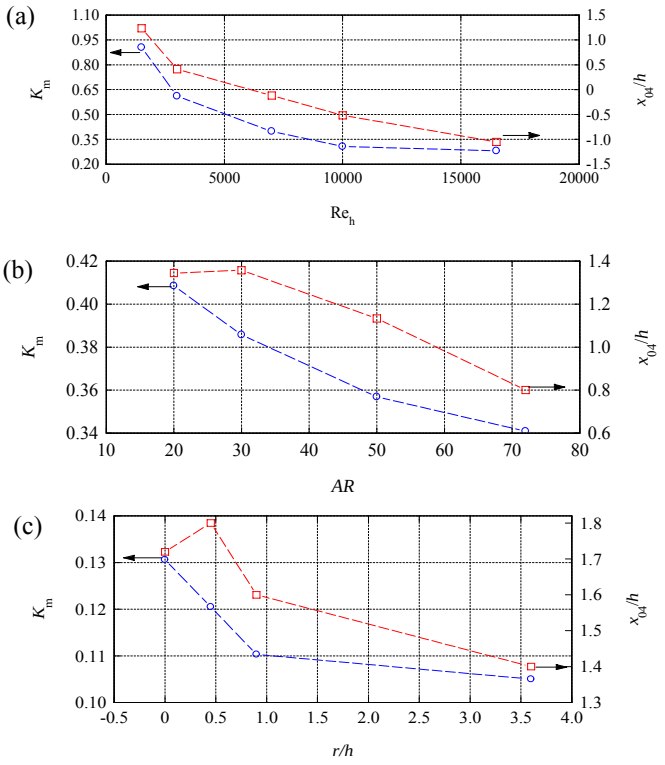


Fig. 4 Effect of nozzle-exit conditions on mass entrainment rates ($K_m$) and virtual origin ($x_{04}/h$) computed using lateral profiles of the mean velocity, $U(x, y)$. (a) $Re$ = 1500 – 16500 ($AR$ = 60, $r^*$= 2.1), (b) $AR$ = 15 – 72 ($Re$ = 18 000, $r^*$ = 3.60), (c) $r^*$= 0 – 3.60 ($Re$ = 18 000, $AR$ = 72)

Fig. 5 displays the growth rates ($K_\delta$) of the outer boundary layer for all prescribed cases. Note that $K_\delta$ has been deduced from the streamwise plot of the displacement thickness stated in (7) (not shown here). Evidently, as $Re$ is increased (Case A), both $K_\delta$ and $x_{05}$ decreases monotonically so that the jet with the lowest $Re$ generates the largest magnitude of $K_\delta$. Likewise, Case C picks up the same trend where the sharp-edged orifice ($r^*$ = 0) produces the largest $K_\delta$. However, the actual magnitude of $K_\delta$ for the lowest Reynolds number ($Re$ =

1500) measure ≈75% that of the orifice case. Noting that the jet with $r^* = 0$ has been measured at a large Reynolds number ($Re$ = 18 000), it is possible that the entrainment rates can be amplified if operating Reynolds number is reduced. Contrary to results for Cases A & C, the magnitudes of $K_\delta$ for Case B follow an opposite trend with increasing $AR$. That is, an increase in aspect ratio is postulated to enhance the growth rate of the boundary layers.

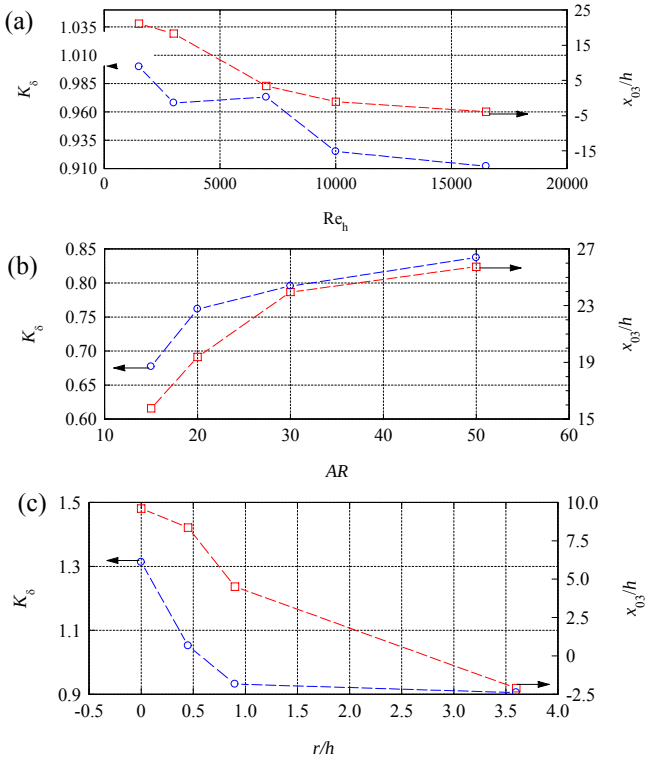


Fig. 5 The effect of nozzle-exit conditions on the growth rate of the shear-layer ($K_\delta$) and virtual origin ($x_{03}/h$) computed from displacement thickness (δ) using lateral profiles of mean velocity, $U(x, y)$. (a) $Re$ = 1500 – 16500 ($AR$ = 60, $r^*$ = 2.1), (b) $AR$ = 15 – 72 ($Re$ = 18 000, $r^*$ = 3.60), (c) $r^*$ = 0 – 3.60 ($Re$ = 18 000, $AR$ = 72)

### *A. Turbulent Flow Properties*

We now investigate the turbulence properties of the prescribed jets using the kinetic energy, $E_k(x) \equiv \frac{1}{2}\langle u_i\rangle\langle u_i\rangle$. In accordance with self-similarity, all planar jets obey

$$E_k(x) = E_{c,\max} \approx \text{ constant at some location, } x_{c,\max} \quad (8)$$

in the near field ($0 \le x/h \le 12$) and

$$E_k(x) = E_{c,\infty} \approx \text{constant at some location } x_{c,\infty} \quad (9)$$

in the self-similar field ($x/h > 20$). Fig. 6 reflects the property represented by (8). For Case A testing jets at various $Re$, the magnitude of $E_{c,\max}/U^2_c$ decreases monotonically with increasing $Re$ so that the low $Re$-jet attains $E_{c,\max}/U^2_c \approx 0.05$ compared to ≈0.02 for the high-$Re$ case. This trend is consistent with the turbulence intensity noted in our earlier study [10]; [22]. It is also found that the location of $E_{c,\max}$ shifts upstream with increasing $Re$.

Case B show that the magnitude of $E_{c,\max}/U^2_c \approx 0.026$ for the jet measured at $AR$ = 15 compared to ≈0.020 for $AR$ = 72 and the location where of this value ($x_{c,\max}$) shifts downstream. Furthermore, a value of $E_{c,\max}/U^2_c \approx 0.039$ is obtained for the orifice-jet compared to ≈0.022 for the contoured case. These distinctions clearly highlight the unique effects manifested by the two kinds of nozzle-exit conditions. The spurt in turbulent kinetic energy for a jet with a low-$Re$ measured from a nozzle with small aspect ratio and a sharp-edged geometry supports more coherent eddy structures [23]. Accordingly, it is deduced that the turbulent kinetic energy in the near field could be enhanced for orifice-jets measured at low $Re$ and high $AR$. Interestingly; it was shown previously (e.g. Fig. 4) that these combinations could enhance the mass entrainment in the far field flow.

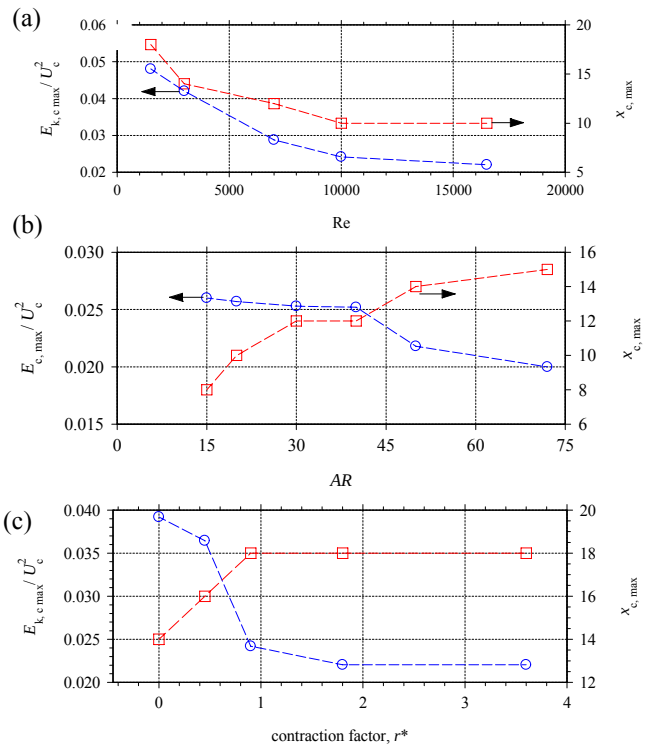


Fig. 6 The effect of nozzle-exit conditions on near-field hump in turbulent kinetic energy ($E_{k\,c,\max}$) and the axial location ($x_{c\,\max}$) this value is noted. (a) $Re$ = 1500 – 16500 ($AR$ = 60, $r^*$ = 2.1), (b) $AR$ = 15 – 72 ($Re$ = 18 000, $r^*$ = 3.60), (c) $r^*$ = 0 – 3.60 ($Re$ = 18 000, $AR$ = 72) (Data recomputed from References [10], part (a); [8], part (b); [7], part (c)

In Fig. 7, the magnitude of the turbulent kinetic energy, $E_{c,\infty}/U^2_c$ in the self-preserving region are plotted. Although the trends of $E_{c,\infty}/U^2_c$ in the far-field for different nozzle profile factors ($r^*$) (Case C) agree with the near-field (Fig. 6), that for Cases A & B ($Re$ & $AR$) follow opposite patterns. Generally, $E_{c,\infty}/U^2_c$ increases with increasing $Re$ and $AR$ so a jet measured at a low Reynolds number with small aspect ratio attains lower

turbulent kinetic energy in the self-similar field. This suggests that a fully turbulent jet issuing from a sharp-edged orifice with high-*AR* is expected to sustain a greater proportion of the turbulent kinetic energy in the self-preserving field.

Fig. 8 displays the probability distribution functions, *PDF* of the velocity fluctuations ($u_c$). To compare the distributions of $u_c$, the *x*-axis is normalized by $<u^2>^{1/2}$ and the Gaussian distribution $p(u_n) = 1/\sqrt{2\pi}\exp\left(-0.5\ln u_n^2\right)$ is shown. There are distinctions between these *PDF*s. From the *x/h* = 5 – 10, very significant departures of the *PDF* from the Gaussian are observed for all cases, and this is especially pronounced for the low-*Re* jet. That is, the lowest-*Re* case exhibits the greatest deviation from the Gaussian distribution. As Reynolds number is increased to 16500, the *PDF* appears to converge. While there appears some difference between the *PDF*s of $u_c$ for jets with different geometric profiles, the role of the nozzle aspect ratio is also evident. For the case of a low-*AR*, the distribution of $u_c$ is skewed to the right side, and this distinction disappears as *AR* is increased to 72.

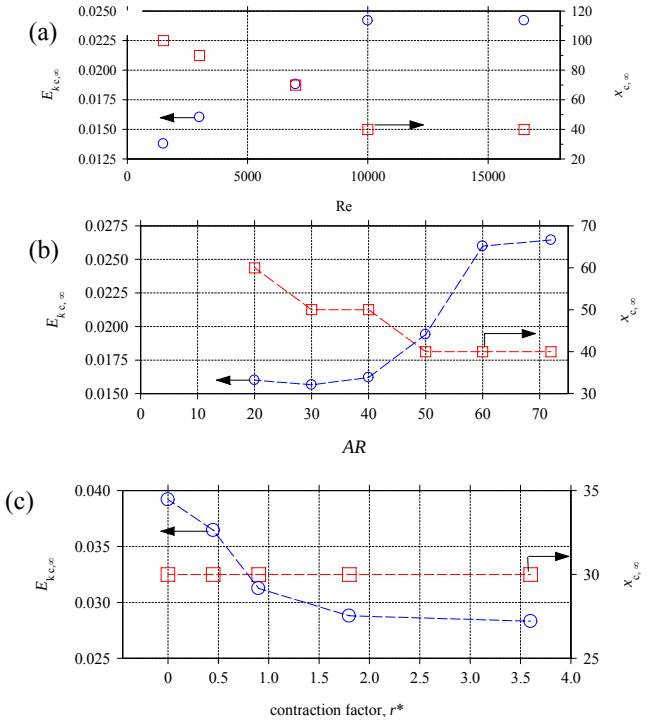


Fig. 7 The effect of nozzle-exit conditions on self-similar value of turbulent kinetic energy ($E_{kc,\infty}$), and the axial location this value is realized ($x_{c,\infty}$). (a) *Re* = 1500 – 16500 (*AR* = 60, *r** of 2.1), (b) *AR* = 15 – 72 (*Re* = 18 000, *r**= 3.60), (c) *r** = 0 – 3.60 (*Re* = 18 000, *AR* = 72) (Data recomputed from References [10], part (a); [8], part (b); [7], part (c)

According to Case C, it is clear that the role of the nozzle aspect ratio on the distribution of $u_c$ appears to be eliminated for *x/h* ≥ 10. In general, the *PDF*s indicate the larger role of the Reynolds number and to a lesser extent, the nozzle aspect ratio in the evolution of the turbulent velocity field. However, between the interaction (*x/h* = 10) and the transition zone (*x/h* = 20), the geometry becomes more significant than that in the near-field (*x/h* ≤10). Finally, in the self-preserving field (*x/h* = 80), role of nozzle-exit conditions seem to decay as all *PDF*s are nearly Gaussian.

### *B. Autocorrelation and Spectral Analysis*

The scale of the large eddy structures ($\Lambda$) is estimated by the auto-correlation function $R_{uu}$ ($\Delta x$, 0, 0) of the fluctuating velocity ($u_c$). By definition, the $R_{uu}$ ($\Delta x$, 0, 0) convolutes the instantaneous velocity signal, *u* at a given point, $x_0$ and given time lag, $\tau = 0$ to another time, $\tau + \Delta\tau$, and displacement $x_0 + \Delta x$.

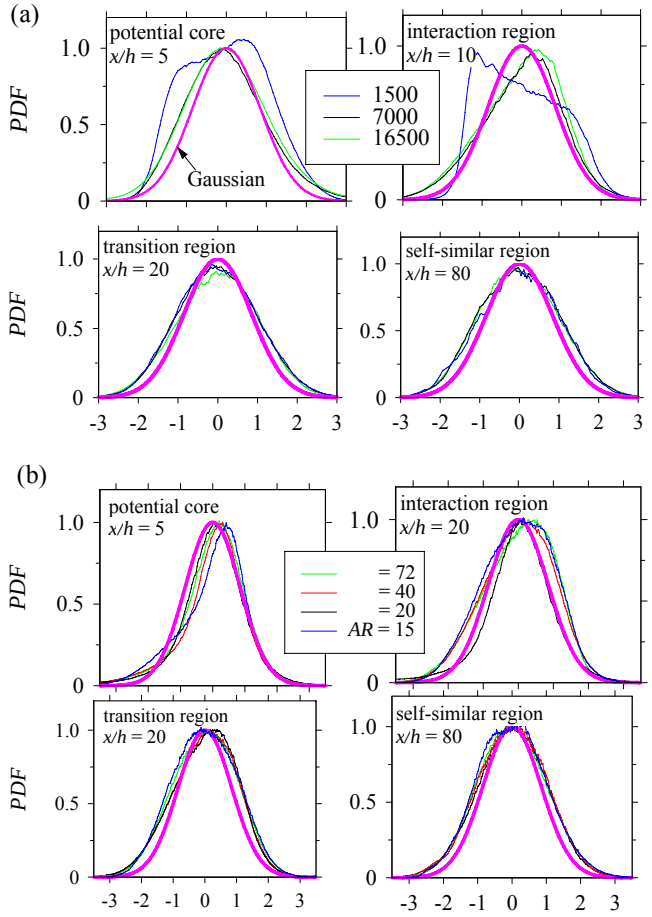

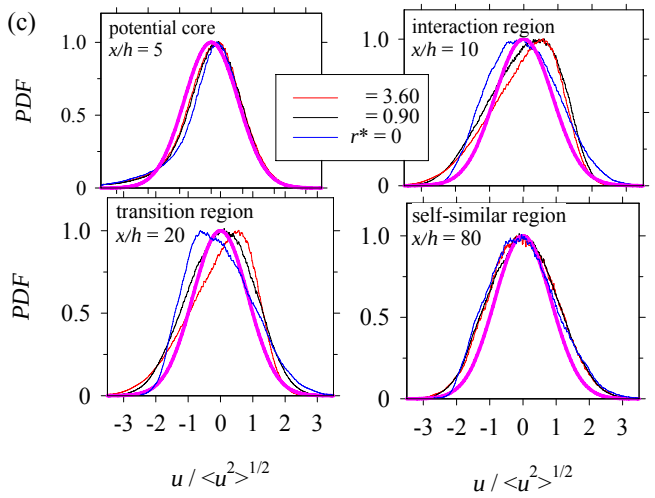


Fig. 8 The probability distribution functions *PDF* of centerline velocity fluctuation in the potential core, interaction, transition and self-similar fields for (a) *Re* = 1500, 7000 and 16500 (*AR* = 60, *r** = 2.1), (b) *AR* = 15 – 72 (*Re* = 18 000, *r** = 3.60), (c) *r** = 0 – 3.60 (*Re* = 18 000, *AR* = 72)

Following Taylor's transformation, $\tau$ is linked to the eddy separation distance ($r = x_0 + \Delta x$) where $r(\Delta x) = U_c\ (x)\ \tau(\Delta t)$. Accordingly, the size of the large eddies ($\Lambda$) is estimated viz

$$\Lambda = \int_{(x=0,R_{uu}=1)}^{(x=\Delta x,R_{u,u}=0)} R_{uu}(\Delta x,0,0)\,d\Delta x \qquad (10)$$

between $\Delta x = 0$ up to the separation distance, $r$ [33]. Fig. 9 (left panel) displays the autocorrelations for the three prescribed cases at $x/h = 3$. For the case with different *Re*, the profiles of $R_{uu}$ follow distinct patterns. The low-*Re* jet exhibits significant oscillation in the amplitude of the autocorrelation function. As the Reynolds is increased, the amplitude of $R_{uu}$ dampens away to resemble those for different *AR* and geometry (middle & bottom panels). Consistent with Fig. 6, the low-*Re* jet encounters greater instabilities in the near-field. Similarly greater instabilities are detected for the jet issuing from the orifice plate with low aspect ratio although these fluctuations can be reduced substantially for the high-*Re* case.

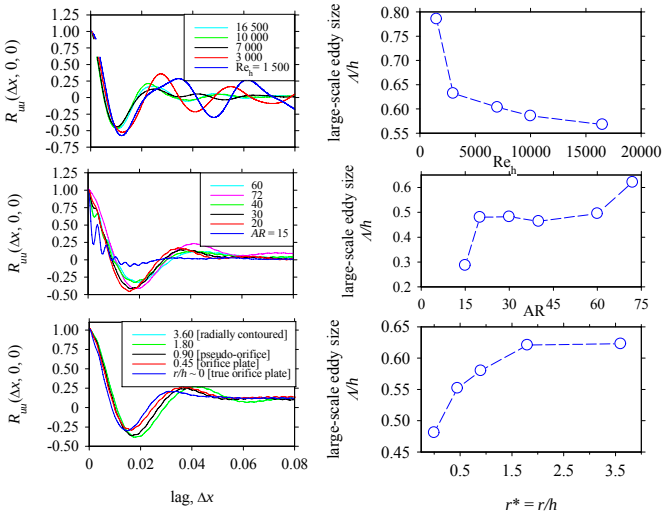


Fig. 9 (a) Left Panel: Autocorrelation function, $R_{uu}$ ($\Delta x$, 0, 0) of velocity fluctuation ($u$); (b) Right Panel: size of large eddies near the potential core ($x/h = 3$)

Some interesting observations are made by checking the magnitude of $\Lambda$ (right panel). It follows that the mean size of the large-scale, coherent eddy structures in the near field are reduced as Reynolds number is increased or both the nozzle aspect ratio and geometric contraction factor is increased. That is, a jet with a low *Re* measured through the orifice plate with a large nozzle aspect ratio will presumably produce larger eddy structures. This contrasts the faster entrainment and jet spreading rate and increased instabilities in the shear layers as noted from the autocorrelation for a low-*AR*-jet measured through an orifice plate. Taken together, Fig. 9 suggests that larger eddy structures could be generated if the Reynolds number is reduced or the nozzle aspect ratio and geometric profile factors are increased.

The properties of the three prescribed jets are investigated by power spectra $\Phi_u(St_h)$ of the fluctuating velocity, $u_c\ (x)$ at $x/h = 3$. The spectra have been obtained by the Fourier transform of $u_c\ (x)$ where $\int_0^\infty \Phi_u(St_h)\,d(St_h) = < u >^2$ and the frequency ($f$) is presented as the Strouhal number, $St_h \equiv fh/U_b$. Consistent with the previous observations [10]–[23], Case A supports an enhanced frequency of large eddy structures with an increase in Reynolds number. This is evidenced by the jet with *Re* = 16500 shedding vortices at a normalized frequency of ≈1.4 times than the jet with *Re* = 1500. This observation stands at odds with Cases B and C where a higher nozzle aspect ratio and larger *r** tends reduce the frequency of large-scale eddy structures. For example, at *AR* = 15, $St_h$ = 0.91 but with an increase in aspect ratio to *AR* = 72, $St_h$ decreases to 0.24. Recall that for *AR* = 15, the autocorrelation function exhibits greater oscillations in the amplitude (Fig. 9 (a)) and a larger jet spreading rate (Fig. 2 (b)). Thus, it is postulated that the increased frequency of vortex shedding for smaller nozzle aspect ratio supports a more unstable shear-layer for this jet.

By contrast, the size of the eddy structures for $AR$ = 15 were presumably smaller than $AR$ = 72 (Fig. 9 (b)).

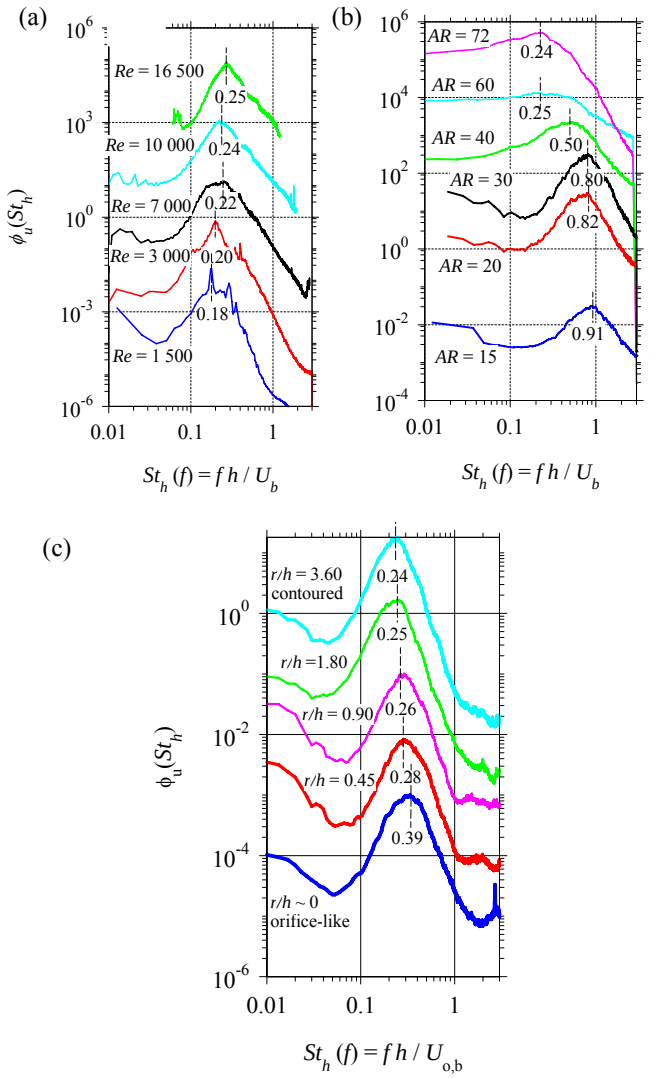


Fig. 10 The power spectral density $\phi_u(St_h)$ versus Strouhal number $St_h = f\,h / U_b$ representing the evolution of primary eddy structures at $x/h$ = 3 for (a) $Re$ = 1500 – 16500 ($AR$ = 60, $r^*$ = 2.1), (b) $AR$ = 15 – 72 ($Re$ = 18 000, $r^*$ = 3.60), (c) $r^*$ = 0 – 3.60 ($Re$ = 18 000, $AR$ = 72)

For Case C, the Strouhal number of the oscillation of vortices for the jet issuing from a sharp-edged orifice geometry ($r^*$ = 0) is ≈1.6 times that of $St_h$ = 0.24 for a jet issuing from a radially contoured geometry. Accordingly, the present analysis shows that the frequency of the large-scale eddy structures in the near field can be amplified for a low-aspect ratio, orifice-jet measured at high Reynolds number.

TABLE II
SUMMARY OF FLOW PROPERTIES

| JET PROPERTY | NEAR-FIELD & INTERACTION ZONE ($0 \le x/h \le 10$) | SELF-PRESERVING (FAR FIELD) ($x/h > 10$) |
|---|---|---|
| Velocity Decay | Highest rate achieved by a nozzle with sharp-edged orifice and low-*AR*, high-*Re* | Highest rate achieved by a nozzle with sharp-edged orifice and high-*AR*, low-*Re* |
| Jet Spreading | | |
| Entrainment (or change of axial mass flux) | Highest rate achieved by a nozzle with sharp-edged orifice and low-*AR*, high-*Re* | Highest rate achieved by a nozzle with sharp-edged orifice and low-*AR*, low-*Re* |
| Boundary Growth (measured by axial displacement thickness) | Not Available | Highest rate achieved by a nozzle with sharp-edged orifice and high-*AR*, low-*Re* |
| Large-scale Eddy Size (measured by integral length scales) | Largest value achieved by a nozzle with radially contoured nozzle with high-*AR*, low-*Re* | Not Available |
| Vortex Shedding Frequency | Most rapid achieved by a nozzle with sharp-edged orifice and low-*AR*, high-*Re* | Not Available |
| Turbulent Kinetic Energy Development | Highest peak value achieved by a sharp-edged orifice and low-*AR*, low-*Re* | Highest asymptotic value sustained by a sharp-edged orifice and high-*AR*, high-*Re* |

## IV. CONCLUDING REMARKS

The mean and turbulent properties of turbulent plane jets measured at different Reynolds number, nozzle aspect ratio and nozzle geometries were reviewed from previous work and additional analysis was conducted to deduce the dominance of any given nozzle-exit condition on the downstream flows. Table II shows that the properties in the near and the far-field. According to the present findings, the decay, spreading, entrainment rates and frequency of large vortices in the near-field is enhanced for the case of a jet issuing from a sharp-edged orifice plate with a low aspect ratio measured at sufficiently high Reynolds number. However, this trend reverses in the far-field where a high nozzle aspect ratio and low Reynolds number is required to produce the same effect.

The turbulent kinetic energy displayed a notable peak around $x/h$ = 10 although the peak was enhanced if the orifice plate was used with a low nozzle aspect ratio and a low Reynolds number jet. By contrast, a jet issuing from the same geometry attained the highest value of far-field turbulent kinetic energy if both the Reynolds number and nozzle aspect ratio were increased. Although the present work is limited to planar jet flows which are not widely used in practical applications, the results may be useful for turbulence modeling and the understanding of net effects of similar initial conditions on downstream behavior of jet flows.

## ACKNOWLEDGMENTS

This research was supported by the Endeavour Research Award, Adelaide Achiever's Award and ARC Linkage Grant under the supervision of Prof. J Mi (Peking University) and GJ Nathan. All experiments were undertaken at the School of Mechanical Engineering (University of Adelaide). Financial support for the international conference travel was provided

by the Faculty Enrichment Fund (FED) at the University of Southern Queensland.

## REFERENCES


[1] A. A. Townsend, *The Structure of Turbulent Shear Flow*, Cambridge University Press, 1956.

[2] W. George, and L. Davidson, L. "Role of initial conditions in establishing asymptotic flow behavior", *American Institute of Aeronautics and Astronautics Journal*, vol 42 (3), pp 438–446, 2004.

[3] W. K. George, "The self-Preservation of turbulent flows and its relation to initial conditions", in *Recent Advances in Turbulence*, Hemisphere, New York, pp 39–73, 1989.

[4] A. K. M. F. Hussain, and A. R. Clark, "Upstream influence on the near field of a planar turbulent jet", *Phys. Fluids*, vol 20(9), 1977.

[5] J. J. Flora, V. W. Goldschmidt, "*Virtual origins of a free plane turbulent jet*", *American Institute of Aeronautics and Astronautics Journal*, vol 7(12), pp 2344–2446, 1969.

[6] R. C. Deo, "*Experimental investigations of the influence of Reynolds number and boundary conditions on a plane air jet*" Ph.D. Thesis, School of Mechanical Engineering, University of Adelaide, Australia, 2005. Available at Australian Digital Thesis Program, http://thesis.library.adelaide.edu.au/public/adt-UA20051025.054550/index.html.

[7] R. C. Deo, J. Mi, and G. J. Nathan, "The influence of nozzle-exit geometric profile on statistical properties of a turbulent plane jet," *Experimental Thermal and Fluid Science*s, vol 32, 545, (2007).

[8] R. C. Deo, J. Mi, and G. J. Nathan, "The influence of nozzle aspect ratio on plane jets," *Experimental Thermal and Fluid Science*, vol 31 (8), pp 825-833, (2007).

[9] R. C. Deo, J. Mi, and G. J. Nathan, "Comparison of turbulent jets issuing from rectangular nozzles with and without sidewalls," *Experimental Thermal and Fluid Sciences*, vol 32, pp 596, (2007).

[10] R. C. Deo, J. Mi, and G. J. Nathan, "The influence of Reynolds number on a plane jet," *Physics of Fluids*, vol 20 (7), pp 075108-1, (2008).

[11] P. R. Suresh, K. Srinivasan, T. Sundararajan, and K. Das Sarit, "Reynolds number dependence of plane jet development in the transitional regime," *Physics of Fluids*, vol 20(4), pp 044105-12, (2008).

[12] G. Heskestad, "Hot-wire measurements in a plane turbulent jet," *Transactions of ASME Journal of Applied Mechanics*, vol 32, pp 721-734, (1965).

[13] L. J. S. Bradbury, "The structure of self-preserving turbulent planar jet" *Journal of Fluid Mechanics*, vol 23, pp 31–64, (1965).

[14] G. P. Lemieux, P. H. Oosthuizen, "Experimental study of behavior of planar turbulent jets at low Reynolds numbers," *American Institute of Aeronautics and Astronautics*, vol 23, pp 1845–1846, (1985).

[15] C. Bogey, and C. Bailly, "Influence of nozzle-exit boundary-layer conditions on the flow and acoustic fields of initially laminar jets," *Journal of Fluid Mechanics*, vol 663, pp 507-538, (2010).

[16] I. Namar, and M. V. Ötügen, "Velocity measurements in a planar turbulent air jet at moderate Reynolds numbers," *Experiments in Fluids*, vol 6, pp 387, (1988).

[17] K. B. M. Q. Zaman, "Far-field noise of a subsonic jet under controlled excitation," *Journal of Fluid Mechanics*, vol 152, pp 83, (1985).

[18] J. Mi, G. J. Nathan, and D. S. Nobes, 'Mixing characteristics of axisymmetric free jets from a contoured nozzle, an orifice plate and a pipe", *ASME Journal of Fluid Engineering*, vol 123, 878–883, 2001.

[19] F. C. Lockwood, and A. Moneib, ''Fluctuating Temperature Measurements in a Heated Round Free Jet,'' *Combustion. Science Technology*, vol 22, pp. 63–81, 1980.

[20] M. Breuer, "A challenging test case for large eddy simulation: high Reynolds number circular cylinder flow', *International Journal of Heat and Fluid Flow*, vol 21, pp 648-654, 2000.

[21] H. Hirovasu, M. Shimizu, and M. Arai. M. "The break-up of high speed jet in a high pressure gaseous atmosphere", in Proc. *The 2nd International Conference on Liquid Atomization and Spray Systems,* Madison, Wisconsin, 1982.

[22] R. C. Deo, G. J., and J. Mi. "Similarity analysis of the momentum field of a subsonic, plane air jet with varying jet-exit and local Reynolds numbers", *Physics of Fluids*, vol 25 (1). pp 015115-1, 2013.

[23] A. Abel-Raheman, "Review of effects of initial and boundary conditions on turbulent jets", *WSEAS transactions on Fluid Mechanics*, vol 5(4), pp 257 – 275, 2010.

[24] B. G. Van Der Hegge Zijnen, 'Measurements of the distribution of heat and matter in a plane turbulent jet of air", *Applied Scientific Research*, vol A7, pp 277–292, 1958.

[25] W. Quinn, "Development of a large-aspect ratio rectangular turbulent free jet", *American Institute of Aeronautics and Astronautics Journal*, vol 32(3), 2007.

[26] H. H. Brunn, *Hot Wire Anemometry: Principles and Signal Analysis*, Oxford Press, 1995.

[27] L. W. B. Browne, R. A. Antonia, S. Rajagopalan, and A. J. Chambers, "Structure of complex turbulent shear flows", *IUTAM Symposium*, Marcseille, pp. 411–419, 1982.

[28] A. J. Chambers, R. A. Antonia, and L. W. B. Browne, "Effect of symmetry and asymmetry of turbulent structures on the interaction region of a plane jet", *Experiments in Fluids* vol 3, 343–348, 1985.

[29] P. Bradshaw, "An introduction to turbulence and its measurements", Pergamon, 1971.

[30] J. Tan-Atichat, W. K. George, and S. Woodward, "Use of Data Acquisition and Processing: Handbook of Fluids and Fluids Engineering", Vol. 3, Wiley, 1996.

[31] C. M. Ho, and E. J. Gutmark "Vortex Induction and Mass Entrainment in a Small-Aspect Ratio Elliptic Jet', *Journal of Fluid Mechanics*, Vol. 179, pp. 383–405, 1987

[32] W. R. Quinn, "Experimental study of the near field and transition region of a free jet issuing from a sharp-edged elliptic orifice plate". *European Journal of Mechanics B/Fluids*, Vol. 26(4), pp. 583-614, 2007.

[33] P. L. O'Neill, D. Nicolaides, D. Honnery, and J. Soria, "Autocorrelation functions and the determination of integral length with reference to experimental and numerical data" in Proc. *The Fifteenth Australasian Fluid Mechanics Conference* (CD-ROM), The University of Sydney, Australia, edited by M. Behnia, W. Lin, and G. D. McBain, (Sydney), 2004.